1,6-Elimination reaction induced detection of fluoride ions in vitro and in vivo based on a NIR fluorescent probe

Aiqing Feng, Yongmei Jia, Liping Huang, Lin Wang, Guohua Zhou, Sheng Wang, Peilian Liu

PII: S1386-1425(19)30489-5
DOI: https://doi.org/10.1016/j.saa.2019.05.013
Reference: SAA 17108
To appear in: *Spectrochimica Acta Part A: Molecular and Biomolecular Spectroscopy*
Received date: 22 November 2018
Revised date: 23 April 2019
Accepted date: 9 May 2019

Please cite this article as: A. Feng, Y. Jia, L. Huang, et al., 1,6-Elimination reaction induced detection of fluoride ions in vitro and in vivo based on a NIR fluorescent probe, Spectrochimica Acta Part A: Molecular and Biomolecular Spectroscopy, https://doi.org/10.1016/j.saa.2019.05.013

1,6-Elimination reaction induced detection of fluoride ions *in vitro* and *in vivo* based on a NIR fluorescent probe

Aiqing Feng [b], Yongmei Jia [a], Liping Huang [a], Lin Wang [c], Guohua Zhou [a], Sheng Wang [a], Peilian Liu [a*]

a. *School of Chemistry and Chemical Engineering, Lingnan Normal University, Zhanjiang 524048, Guangdong, PR China*

b. *Department of Life Science, Luoyang Normal University, Luoyang 471934, PR China*

c. *Analytical and Testing Center, Jinan University, Guangzhou 510632, PR China*

Corresponding Author

Tel.: 86-759-3183176. Fax: 86-759-3183176. E-mail address: liupeilian2010@126.com

ABSTRACT

Near-Infrared "turn on" type fluorescent probes are attractive and promising in the fields of chemical sensing and bioimaging. Here, a new dicyanomethylene-4H-pyran derivative (DCM-Si) NIR fluorescent probe was designed and synthesized for specific lighting up F^- in living cells and bodies. Si-O bond was used as F^- trigger, and the release of fluorophore ($DCM\text{-}NH_2$) occurred after substituent reaction and subsequent 1,6-elimination. This NIR probe displayed high sensitivity and selectivity for the sensing of F^-, and the detection limit was calculated to be as low as 157 nM. Moreover, the "off-on" fluorescent signal changes can be realized by adding F^- in living cells and zebrafish embryos.

Keywords: 1,6-elimination; fluoride ions; fluorescent probe; NIR

1. Introduction

The development and synthesis of fluorescent probes for sensing anions in biologically and chemically relevant conditions have attracted much attention [1-11]. Fluoride is considered as a special ion due to its dual natural properties in biological science. Appropriate intake of fluoride can reduce the risk of dental caries, but the excessive fluoride will bring some diseases including dental and skeletal fluorosis, and even cause kidney failure [12-16]. Therefore, it is very necessary to explore sensors for accurate monitoring fluoride ions in drinking water as well as in living species. Although ion-selective electrode and ion chromatography have been considered as the standard lab methods to detect F^- quantitatively, the required equipment and facilities are tedious and expensive [17,18]. In recent years, the fluorescent probes for F^- have attracted more attention because they provide a highly selective, sensitive and convenient strategy in real sample testing [19-27]. However, most conventional probes display short emissive wavelength (in the UV or visible range) that greatly limit their application in living cells and *in vivo*.

In the past decade, near-infrared (NIR) fluorescent probes have received much attention because of their unique optical performances including weaker fluorescence background, lower photobleaching, and strong photon penetration depth [28-33]. Many NIR fluorescent probes have been designed, prepared, and applied for detecting and imaging various important analytes (such as proteins and active radicals) in the field of biology [34-38]. Generally, the mechanism of sensing for F^- can be divided into three interacted types: hydrogen bonding, boron-fluoride complexation, and Si-O cleavage [39-44]. Although some NIR probes have been reported for the detection of F^- in aqueous solution or living cells based on

fluoride-mediated desilylation strategy, few of them can be applicated for F^- imaging *in vivo* [45].

In this paper, a new fluoride-activatable NIR fluorescent probe (DCM-Si) was designed and synthesized for the detection of F^- *in vitro* and *in vivo*. As shown in Scheme 1, DCM-Si containing a Si-O linking erasable group as fluorescence quencher and specific fluoride trigger for minoring F^- in living cells and zebrafish based on the cleavage of Si-O bond followed by 1,6-elimination to release DCM-NH_2. As expected, a "turn on" fluorescent emission of DCM-Si located at 665 nm was observed upon adding F^-, which providing a strong broad band in the near infrared region. Moreover, further studies proved the DCM-Si with low cytotoxicity was suitable to track F^- level elevation in living cells and zebrafishes through fluorescent imaging technology.

2. Experimental section

2.1. Materials

(2-Hydroxy-5-methyl-1,3-phenylene) dimethanol (98%), 2-iodylbenzoic acid (97%), ethyl 2-(triphenylphosphoranylidene) acetate (98%), tert-butylchlorodimethylsilane (TBSCl, 99%), triethylamine (AR), diisobutyl aluminium hydride (1.5 M in toluene), tert-butoxycarbonyl anhydride (98%), trifluoroacetic acid (AR), and triphosgene (98%) were purchased from Energy Chemical, Shanghai, China. Tetrabutylammonium fluoride (1 M in THF), tetrabutylammonium chloride (98%), tetrabutylammonium bromide (99%), tetrabutylammonium iodide (99%), tetrabutylammonium acetate (97%), tetrabutylammonium hydrogen sulfate (98%), tetrabutylammonium phosphate (99%), tetrabutylammonium nitrate (98%), and tetrabutylammonium hydroxide (1M in MeOH) were purchased from Aladdin

Chemistry Co. Ltd.. All used organic solvents were purchased from Guangzhou Chemical Reagent Factory and used without further purification.

2.2. Apparatus

UV-Vis spectra were recorded on TECHCOMP spectrophotometer in the range of 320-750 nm with a slit of 2 nm. Fluorescence and excitation spectra were measured using a Hitachi F-7000 fluorescence spectrophotometer with a 150 W xenon lamp as a light source. ^{1}H NMR and ^{13}C NMR spectra were recorded on a Bruker 400 MHz NMR Spectrometer. HPLC analyses were performed on Agilent 1260. Cells imaging experiments were carried out on a Leica TCS SP5 CLSM using 488 nm laser as the excitation light source. The fluorescence images of zebrafish were afforded by an Olympus IX 71 fluorescence microscope with a DP72 color CCD.

2.3. Synthesis of the probe

Synthesis of compound **1**: To a solution of (2-hydroxy-5-methyl-1,3-phenylene) dimethanol (1 g, 5.95 mmol) in ethyl acetate (20 mL) was added 2-iodylbenzoic acid (5 g, 17.86 mmol). The mixture solution was stirred under refluxing for 3 h. After filtrating the solid, the filtrate was evaporated to obtain the crude product. Then, the product was purified by column chromatography on silica gel to obtain the target compound as a white solid (yield: 76.3%). ^{1}H NMR (400 MHz, $CDCl_3$, ppm): 11.47 (s, 1H), 10.23 (s, 2H), 7.78 (s, 2H), 2.40 (s, 3H).

Synthesis of compound **2:** Compound **1** (745 mg, 4.54 mmol) and ethyl 2-(triphenylphosphoranylidene) acetate (6.3 g, 18.1 mmol) were dissolved in dichloromethane (30 mL), and the mixture was stirring under room temperature for 6 h. The organic solvent

was removed by decompression. Then, the crude product was purified by column chromatography on silica gel to afford the compound **2** as a white solid (yield: 86.4%). ^{1}H NMR (400 MHz, $CDCl_3$, ppm): 8.10-8.20 (d, 2H), 7.35 (s, 2H), 6.45-6.55 (d, 2H), 4.25-4.40 (m, 4H) 2.32 (s, 1H), 1.30-1.40 (t, 6H), 1.27 (s, 1H). ^{13}C NMR (101 MHz, $CDCl_3$, ppm): 167.68, 152.01, 139.47, 130.42, 129.99, 123.01, 119.15, 60.82, 20.52, 14.33.

Synthesis of compound **3:** Compound **2** (0.5 g, 4.54 mmol) was dissolved in 30 mL of dichloromethane, and 10 eq. of triethylamine was added into the solution. Subsequently, tert-butylchlorodimethylsilane (1.739 g, 7 eq.) was added into the mixture carefully. After stirring under room temperature for 6 h, the mixture was diluted with a certain amount of dichloromethane, and washed with DI water three times. The organic phase was first dried by anhydrous sodium sulfate, and then removed under vacuum to obtain the crude product. The product was purified by column chromatography on silica gel to afford the compound **3** as a yellow powder (yield: 95.9%). ^{1}H NMR (400 MHz, $CDCl_3$, ppm): 7.85-8.00 (d, 2H), 7.41 (s, 2H), 6.32-4.36 (d, 2H), 4.23-4.35 (m, 4H), 2.32 (s, 1H), 1.32-1.35 (t, 6H), 1.11 (s, 9H), 0.12 (s, 6H). ^{13}C NMR (101 MHz, $CDCl_3$, ppm): 166.89, 151.29, 140.03, 131.41, 129.32, 126.99, 118.03, 60.49, 25.89, 20.73, 18.50, 14.34, -3.82.

Synthesis of compound **4:** Compound **3** (650 mg, 1.55 mmol) was sealed up within the round bottom flask (100 mL), then tetrahydrofuran (30 mL) was added into the bottom under the protection of nitrogen gas. After cooling down to -78℃, diisobutyl aluminium hydride (20.7 mL) was drop into the reaction bottle slowly in about 45 min, and the mixture was stirring for 1 h. Then, the temperature was slowly heated up to room temperature, and the mixture was reacted for further 1 h. 20 mL water was slowly drop into the bottle to quench the

reaction. The solution was extracted with ethyl acetate three times, then the organic phase was combined and dried by anhydrous sodium sulfate overnight. The purified compound **4** with yellow color was obtained by column chromatography on silica gel (yield: 97.6%). ^{1}H NMR (400 MHz, DMSO-d_6, ppm): 7.21 (s, 2H), 6.73-6.78 (d, 2H), 6.20-6.26 (m, 2H), 4.10-4.12 (m, 4H), 2.24 (s, 3H), 1.01 (s, 9H), 0.07 (s, 6H). ^{13}C NMR (101 MHz, DMSO-d_6, ppm): 147.68, 130.95, 130.73, 129.02, 125.92, 124.50, 62.17, 26.44, 20.90, 18.71, -2.99.

Synthesis of compound **5:** DCM-NH_2 (68 mg, 0.22 mmol) and triphosgene (194.8 mg, 0.66 mmol) were added into the 25 mL of round bottom flask under the protection of nitrogen. After being dissolved by dichloromethane (9 mL), the solution was cooled to 0 ℃. 3 mL of dichloromethane containing pyridine (158.2 μL, 1.97 mmol) was added into the bottom slow down with a syringe. After stirring at 0 ℃ for 1 h, the mixture was keeping further 2 h at room temperature. Dichloromethane was removed by decompression under room temperature. 10 mL dichloromethane solution of compound **4** (220.5 mg, 0.22 mmol) was rapidly into the bottom under the protection of nitrogen gas. The mixture was stirring under room temperature overnight. The solvent was removed under vacuum to obtain the crude product. The product was purified by column chromatography on silica gel to obtain the compound **5** as a yellow solid (yield: 48.3%). ^{1}H NMR (400 MHz, $CDCl_3$, ppm): 8.93-8.95 (m, 1H), 7.74-7.78 (m, 1H), 7.46-7.63 (m, 7H), 7.23-7.24 (d, 2H), 6.74-6.99 (m, 6H), 6.20-6.30 (m, 2H), 4.86-4.88 (d, 2H), 4.33-4.35 (d, 2H), 2.31 (s, 3H), 1.08(s, 9H), 0.12 (s, 6H). ^{13}C NMR (101 MHz, DMSO-d_6, ppm): 157.66, 152.87, 152.92, 152.34, 148.41, 140.04, 138.30, 134.61, 131.04, 130.57, 129.73, 129.11, 128.77, 128.25, 128.12, 127.38, 126.99, 126.50, 125.95, 125.85, 122.47, 118.68, 118.58, 117.87, 117.30, 116.90, 115.82, 106.60, 66.40, 64.10, 62.43, 29.72, 26.03,

20.80, -3.36.

2.4. The procedure for spectral analysis

All absorption and emission spectra of DCM-Si were carried out in DMSO containing 5% H_2O. 100 μL of water, 1.88 mL of DMSO, and 20 μL DMSO stock solution of DCM-Si (0.5 mM) were added into a 2 mL tube to afford the final concentration (5 μM). Tetrabutylammonium salt including (F^-, Cl^-, Br^-, I^-, AcO^-, HSO_4^-, $H_2PO_4^-$, NO_3^-, or OH^-) was dissolved in DMSO, and an appropriate volume was added to the sample solution. Then, the solution was transferred into a 10×10 mm quartz cuvette to conduct the measurement of absorption and fluorescence spectra.

2.5. DFT calculations

The nature of the ground states (HOMO) and singlet excited states (LUMO) of DCM-Si and DCM-NH_2 was calculated by quantum chemistry theory. The geometry optimization and energy level for samples were displayed by the method of the density functional theory (DFT) at the B3LYP level using a suite of Gaussian 09 programs [46,47].

2.6. Cell culture.

Human epithelioid cervical carcinoma cell line (HeLa cells) was used in this study. Cells were cultured in Dulbecco's modified medium (DMEM) supplemented with 10% fetal bovine serum and 1% antibiotics penicillin at 37 °C under 5% CO_2 atmosphere.

2.7. Cell viability assay

To explore the cytotoxicity of DCM-Si, the HeLa cells were cultured at 37 °C with 5% CO_2 and grown for one day. After removal of the medium, cells were cultured with standard medium containing various concentrations of F^- (0, 5, 10, 15, 20, 25, or 30 μM) for further

one day. The cytotoxicity of DCM-Si was evaluated by MTT assay based on ISO 1099. Each sample was performed in five replicates, and the cell viability was performed by the statistical mean and standard deviation.

2.8. Cell imaging

The HeLa cells were plated on polylysine-coated cell culture glass slides inside the 30 mm glass culture dishes and allowed grown to 70% confluency. After washing with DMED medium, cells were cultured with various amount F^- (0, 50, and 100 μM, respectively) at 37 °C under 5% CO_2 for 60 min. Cells were washed with medium again prior to incubate with the medium containing DCM-Si (10 μM) and 0.5% DMSO for another 60 min. Subsequently, we picked up the glass slides, and washed the cells by PBS buffer for three times. Finally, the cells were imaged on a Leica TCS SP5 CLSM with a blue laser (λ_{ex} = 488 nm), and the fluorescent signal collection wavelength was 620 to 720 nm.

2.9. Zebrafish imaging

Zebrafish embryos of the pharyngula period (48 hpf) were incubated with E3 media (15 mM NaCl, 0.5 mM KCl, 1 mM $MgSO_4$, 1 mM $CaCl_2$, 0.15 mM KH_2PO_4, 0.05 mM Na_2HPO_4, 0.7 mM $NaHCO_3$; pH 7.5) containing DCM-Si (20 μM) and 0.5% DMSO for 4 h. The zebrafishes were washed with E3 media three times prior to imaging. As for the fluoride ions imaging, two groups were further cultured with 50 and 100 μM of F^- for another 1h, respectively.

3. Result and discussion

3.1 Synthesis of the probe (DCM-Si)

Scheme 2 illustrated the synthetic route of DCM-Si. The two benzyl alcohol groups of

(2-hydroxy-5-methyl-1,3-phenylene) dimethanol were oxidized to aldehyde groups by adding the oxidant (2-iodylbenzoic acid) into the reaction system, and the crude product was purified to form compound **1**. Compound **1** was reacted with ethyl 2-(triphenylphosphoranylidene) acetate via Witting reaction to form compound **2**. The phenolic hydroxyl of compound **2** was allowed to react with TBSCl to afford compound **3**. Then, the carboxylate esters were reduced by diisobuty aluminium hydride to alcohols at low temperature (-78 ℃) to yield compound **4**. Finally, DCM-NH_2 [48] was bonded with compound **4** using triphosgene to obtain the target probe compound **5** (DCM-Si). Compound **1-5** were well characterized by ^{1}H and ^{13}C nuclear magnetic resonance (Figs. S3-S11).

3.2 UV response of DCM-Si toward F^-

The UV spectra of DCM-Si in the presence or absence of F^- were investigated. As shown in Fig. S1, the prepared NIR probe DCM-Si has a broad absorption band (centered at 455 nm) with the range from 350 to 625 nm, which is attributed to the existence of the intramolecular charge transfer (ICT) in the conjugate system. This peak was dramatically reduced in the presence of F^-, and a new absorption peak appeared at 516 nm which was almost at the same location for the free DCM-NH_2. This phenomenon might due to the reaction between F^- and DCM-Si to form DCM-NH_2. Some similar anions including Cl^-, Br^-, I^-, AcO^-, HSO_4^-, $H_2PO_4^-$, NO_3^-, and OH^- were added into the solution of DCM-Si, respectively. There was almost no obvious change in the UV absorption curves, proving that the NIR probe can distinguishing the fluoride ion selectively. Furthermore, the response time of DCM-Si toward F^- was also studied. The maximum absorption wavelength of DCM-Si was red shift range from 455 nm to 516 nm with the increasing time exposing to the F^- in the solution (Fig. 1). As time goes on,

the obviously color change from yellow to pink was observed, which provided the colorimetric recognition for F^- directly by naked eye (Figure 1, inset photo).

3.3 Fluorescent response of DCM-Si toward F^-

The fluorescent spectra of DCM-Si (5 μM) toward F^- in DMSO aqueous solution (water/DMSO = 5/95, v/v) at room temperature (λ_{ex} = 480 nm) were investigated. As shown in Fig. 2, DCM-Si exhibited the faint emission with the maximum wavelength at 570 nm. Upon adding 20 eq. of F^- (100 μM) into the DCM-Si solution, the peak located at 570 nm was dramatically decreased, while a new emission band located at 665 nm was occurred and continuous to enhance with the increasing time. These results displayed the silicon oxygen bond of DCM-Si was broke successfully in the presence of F^-, and the 1,6-elimination reaction was occurred subsequently. The totally process was almost done in 40 min. And we therefore clearly observed the fluorescence color changes of DCM-Si from dark to red under the irradiation of ultraviolet lamp (Fig. 2, inset photo).

In addition, the quantitative detection ability of DCM-Si for fluorine ion was evaluated by using the fluorescence titration experiments. After exposing to different concentrations of F^- (0 - 100 μM) with 40 min, the emission intensities of DCM-Si significantly increased and almost reached a balance at the 100 μM of F^- (Fig. 3). The scatter plot of the relative intensity of DCM-Si at 665 nm versus the concentration of F^- was investigated in Fig. 3 inset photo. The fluorescence intensity increased rapidly until the concentration of fluoride reached 50 μM, and became slow afterward. Interestingly, the emission intensity change ($F-F_0$) versus the F^- concentration range from 1 to 40 μM followed a simple linear equation $y = 40.77x - 36.23$ ($R^2 = 0.998$), and the detection limit (DL) of DCM-Si for F^- had been calculated as 157 nM by the

equation DL = 3SD / slope, where SD is the standard deviation of the blank signal of DCM-Si (n=5) (Fig. 4).

The selectivity of DCM-Si toward F^- was also evaluated by the fluorescence emission spectra of the NIR probe in the presence of fluorine ion or some other similar anions (Cl^-, Br^-, I^-, AcO^-, HSO_4^-, $H_2PO_4^-$, NO_3^-, OH^-). As shown in Fig. 5, adding F^- into the DCM-Si solution could induce significant enhancement of the emission curve, while almost no change was observed in the presence of the other analytes. Moreover, the selectivity performance of DCM-Si under the coexistence of F^- and other analytes was also explored. DCM-Si can still make a specific response for F^- in the mixture of coexisting ions at the same concentration. All these results therefore proved that the NIR probe based on DCM-Si was selective for sensing fluoride ions.

3.4 Mechanism of DCM-Si responding to F^-

To investigate the detecting mechanism, the data was collected for the standard DCM-NH_2, and DCM-Si in presence or absence of F^- using the HPLC method. As shown in Fig. 6, upon adding 10 eq. of F^-, the peak located at 3.909 mins of DCM-Si was disappeared, and a new peak was observed at 2.801 min which was consistent with the retention time of DCM-NH_2. This result clearly showed that the increasing of the fluorescence intensity was caused by the release of DCM-NH_2. Before treating with F^-, the fluorescence of the DCM moiety was quenched through the weaker intramolecular charge transfer (ICT) process to ensure a low fluorescence background in the probe. Upon addition of F^-, the silicon oxygen bond of DCM-Si was cleavage to generate a phenolic-hydroxyl containing intermediate which was chemically labile and underwent a 1,6-elimination spontaneously to release DCM-NH_2

concomitantly, and thus lead to the fluorescence turn-on process due to the strong ICT. The sensing mechanism of DCM-Si toward F^- was depicted in Scheme 1. In fact, the identical absorption spectra of DCM-Si and DCM-NH_2 also proved that the Si-O bond of DCM-Si was cracked to release DCM-NH_2 with the treatment of F^- (Fig. S1).

Density functional theory (DFT) calculations were evaluated for the electron density of DCM-Si and DCM-NH_2 at the B3LYP level through the Gaussian 09 package. As for the NIR probe DCM-Si, the electron density mainly located at the benzene ring linked with siloxane in its HOMO orbital, and the electron transfer occurred to the benzopyran unit in its lowest unoccupied molecular orbital (LUMO) (Fig. 7). Compared with the band gap of DCM-Si (2.973 ev), the smaller band gap (2.902 ev) of DCM-NH_2 can explain the red shift of maximum absorption (from 455 nm to 516 nm) and fluorescence emission (from 570 nm to 665 nm) of the probe with the treatment of F^- (Fig. S1 and Fig. 2).

3.5 Detection ability of DCM-Si in vitro

To evaluate the detection ability of the probe toward F^- within living cells, HeLa cell line was chosen to study the cytotoxicity of DCM-Si by MTT assay. As shown in Fig. S2, the cell mortality rate was lower than 10% upon respective treatment with high concentration of DCM-Si (30 μM) for 24 h, indicating that DCM-Si possessed good biocompatibility, and could be utilized as a NIR "*off-on*" type probe for sensing F^- in live cells. In addition, the HeLa cells were also used for exploring the cell imaging capability of DCM-Si with various concentrations of F^- by confocal laser scanning microscope (Fig. 8). No obvious signal in red channel was observed from cells treated with DCM-Si (10 μM) for 60 min (A). In contrast, the cells displayed NIR fluorescence signal in the same channel upon being precultured with

F^- (50 μM) for 60 min and then incubated with DCM-Si (10 μM) for further 60 min (B). The red was enhanced depending on the changes in concentration of the preincubated F^- (100 μM, C), indicating that DCM-Si not only had excellent cell membrane permeability, but also could be activated by the fluorine ions inside cells. Therefore, this novel low toxic NIR fluorescence probe would offer an efficient way for tracking F^- in biological systems.

3.6 Detection ability of DCM-Si in vivo

Zebrafish was displayed as the animal model to demonstrate that the fluorescence imaging of F^- in vivo could be tracked by DCM-Si, as the zebrafish possessed many advantages (such as excellent optical transparency, high fecundity, external fertilization, and so on.). Zebrafishes were incubated with free DCM-Si (10 μM) as a control group, and another two groups were stained with DCM-Si (10 μM) for a certain amount of time prior treating with 50 and 100 μM F^- separately. As shown in Fig. 9, there was no fluorescence signal observed in the control experiment treating without F^- (A). The obviously red fluorescence located at the yolk of embryo was obtained with the addition of F^- (50 μM, B), and the emission of yolk was increased with the higher concentration of F^- (100 μM, C). Combined with the behavior of DCM-Si in vivo, it can be clearly concluded that the Si-O bond of DCM-Si was successful broke by F^- in living bodies.

4. Conclusions

In summary, we have reported a novel "*off-on*" NIR fluorescent probe by utilizing the inhibition of intramolecular charge transfer (ICT). DCM-Si exhibits almost no fluorescent emission in terms of ICT block from the amino group of DCM-NH_2. When adding F^-, the Si-O bond of DCM-Si is substituted to the form of phenolic hydroxyl, and the 1,6-elimination

can subsequently be spontaneously to release DCM-NH_2 concomitantly with the NIR fluorescence (at 665 nm) turn-on process due to the strong ICT from amino group. Notably, DCM-Si is successfully applied for the quantitative sensing of exogenous fluoride ions in HeLa cells and zebrafish embryos through the fluorescence imaging.

Acknowledgements

The work was supported by Natural Science Foundation of Guangdong Province (2017A030310604; 2018A030307035; 2016A030310362; 2018A030307037; 2014A030310274), Guangdong University Provincial Key Platform and Major Research Projects: Characteristic Innovation Project (2017KTSCX118), Natural Science Foundation of Lingnan Normal University (ZL1802), and National Natural Science Foundation of China (21878136).

References

[1] D. Wu, A.C. Sedgwick, T. Gunnlaugsson, E.U. Akkaya, J. Yoon, T.D. James, Fluorescent chemosensors: the past, present and future, Chem. Soc. Rev. 46 (2017) 7105-7123.

[2] P. Molina, F. Zapata, A. Caballero, Anion recognition strategies based on combined noncovalent interactions, Chem. Rev. 117 (2017) 9907-9972.

[3] L. Wu, I.C. Wu, C.C. DuFort, M.A. Carlson, X. Wu, L. Chen, C.T. Kuo, Y. Qin, J. Yu, S.R. Hingorani, D.T. Chiu, Photostable ratiometric Pdot probe for in vitro and in vivo imaging of hypochlorous acid, J. Am. Chem. Soc. 139 (2017) 6911-6918.

[4] Z. Zhou, X.Q. Li, Y.P. Tang, C.C. Zhang, H.R. Fu, N.T. Wu, L.F. Ma, J.W. Gao, Q.M. Wang, Oxidative deoximation reaction induced recognition of hypochlorite based on a

new fluorescent lanthanide-organic framework, Chem. Eng. J. 351 (2018) 364-370.

[5] Y.L. Wu, J. Wang, F. Zeng, S.L. Huang, J. Huang, H.T. Xie, C.M. Yu, S.Z. Wu, Pyrene derivative emitting red or near-infrared light with monomer/excimer conversion and its application to ratiometric detection of hypochlorite, ACS Appl. Mater. Interfaces 8 (2016) 1511-1519.

[6] Z. Zhou, M.L. Han, H.R. Fu, L.F. Ma, F. Luo, D.S. Li, Engineering design toward exploring the functional group substitution in 1D channels of Zn-organic frameworks upon nitro explosives and antibiotics detection, Dalton Trans. 47 (2018**)** 5359-5365.

[7] B. Yan, Lanthanide-functionalized metal-organic framework hybrid systems to create multiple luminescent centers for chemical sensing, Acc. Chem. Res. 50 (2017) 2789-2798.

[8] X.Q. Li, Z. Zhou, C.C. Zhang, Y.H. Zheng, J.W. Gao, Q.M. Wang, Ratiometric fluorescence platform based on modified silicon quantum dots and its logic gate performance, Inorg. Chem. 57 (2018) 8866-8873.

[9] Y. Li, X.L. Xie, X.E. Yang, M.M. Li, X.Y. Jiao, Y.H. Sun, X. Wang, B. Tang, Two-photon fluorescent probe for revealing drug-induced hepatotoxicity via mapping fluctuation of peroxynitrite, Chem. Sci. 8 (2017) 4006-4011.

[10] Z. Zhou, C.C. Zhang, Y.H. Zheng, Q.M. Wang, Luminescence modulation of two individual fluorophores over a wide pH range and intracellular studies, Dyes Pigments 150 (2018) 151-157.

[11] J.L. Kolanowski, F. Liu, E.J. New, Fluorescent probes for the simultaneous detection of multiple analytes in biology, Chem. Soc. Rev. 47 (2018) 195-208.

[12] X.X. Chen, T.H. Leng, C.Y. Wang, Y.J. Shen, W.H. Zhu, A highly selective naked-eye

and fluorescent probe for fluoride ion based on 1,8-naphalimide and benzothizazole, Dyes Pigments 141 (2017) 299-305.

[13] A. Roy, D. Kand, T. Saha, P. Talukdar, A cascade reaction based fluorescent probe for rapid and selective fluoride ion detection, Chem. Commun. 50 (2014) 5510-5513.

[14] X. Yuan, X.J. Xu, C.X. Zhao, F. Zhang, Y.X. Lu, Y.J. Shen, C.Y. Wang, A novel colorimetric and fluorometric fluoride ion probe based on photoinduced electron transfer signaling mechanism, Sens. Actuator B-Chem. 253 (2017) 1096-1105.

[15] S.K. Padhan, M.B. Podh, P.K. Sahu, S.N. Sahu, Optical discrimination of fluoride and cyanide ions by coumarin-salicylidene based chromofluorescent probes in organic and aqueous medium, Sens. Actuator B-Chem. 255 (2018) 1376-1390.

[16] D. Kim, S. Singha, T. Wang, E. Seo, J.H. Lee, S.J. Lee, K.H. Kim, K.H. Ahn, In vivo two-photon fluorescent imaging of fluoride with a desilylation-based reactive probe, Chem. Commun. 48 (2012) 10243-10245.

[17] P. Konieczka, B. Zygmunt, J. Namiesnik, Comparison of fluoride ion-selective electrode based potentiometric methods of fluoride determination in human urine, B. Environ. Contam. Tox. 64 (2000) 794-803.

[18] Y. Mlchlganu, Y. Kuroda, K. Ueda, Y. Yamamoto, Determination of urinary fluoride by ion chromatography. Anal. Chim. Acta *274* (1993) 299-302.

[19] P. Sokkalingam, C.H. Lee, Highly sensitive fluorescence "turn-on" indicator for fluoride anion with remarkable selectivity in organic and aqueous media, J. Org. Chem. 76 (2011) 3820-3828.

[20] P. Hou, S. Chen, H.B. Wang, J.X. Wang, K. Voitchovsky, X.Z. Song, An aqueous red

emitting fluorescent fluoride sensing probe exhibiting a large Stokes shift and its application in cell imaging, Chem. Commun. 50 (2014) 320-322.

[21] I.S. Turan, E.U. Akkaya, Chemiluminescence sensing of fluoride ions using a self-immolative amplifier, Org. Lett. 16 (2014) 1680-1683.

[22] X.K. Tian, J.H. Wang, Y. Li, C. Yang, L.Q. Lu, Y.L. Nie, Sensitive determination of hardness and fluoride in ground water by a hybrid nanosensor based on aggregation induced FRET on and off mechanism, Sens. Actuator B-Chem. 262 (2018) 522-530.

[23] Z.R. Yang, M.M. Wang, X.S. Wang, X.B. Yin, Boric-acid-functional lanthanide metal-organic frameworks for selective ratiometric fluorescence detection of fluoride ions, Anal. Chem. 89 (2017) 1930-1936.

[24] S.Y. Chen, H. Yu, C. Zhao, R. Hu, J. Zhu, L. Li, Indolo[3,2 -b]carbazole derivative as a fluorescent probe for fluoride ion and carbon dioxide detections, Sens. Actuator B-Chem. 250 (2017) 591-600.

[25] K. Dhanunjayarao, V. Mukundam, K. Venkatasubbaiah, A highly selective ratiometric detection of F^- based on excited-state intramolecular proton-transfer (imidazole) materials, J. Mater. Chem. C 2 (2014) 8599-8606.

[26] P. Ghosh, N. Kumar, S.K. Mukhopadhyay, P. Banerje, Sensitive and fluorescent Schiff base chemosensor for picomolar level fluoride detection: In vitro study and mimic of logic gate function, Sens. Actuator B-Chem. 224 (2016) 899-906.

[27] A.R. Chowdhury, P. Ghosh, B.G. Roy, S.K. Mukhopadhyay, N.C. Murmu, P. Banerjee, Cell permeable fluorescent colorimetric Schiff base chemoreceptor for detecting F^- in aqueous solvent, Sens. Actuator B-Chem. 220 (2015) 347-355.

[28] Z.Q. Guo, T.G. Ma, Y.J. Liu, C.X. Yang, P. Shi, H. Tian, W.H. Zhu, Photocaged prodrug under NIR light-triggering with dual-channel fluorescence: in vivo real-time tracking for precise drug delivery, Sci. China Chem. 61 (2018) 1-8.

[29] K.Y. Liu, H.M. Shang, X.Q. Kong, W.Y. Lin, A novel near-infrared fluorescent probe with a large stokes shift for biothiol detection and application in in vitro and in vivo fluorescence imaging, J. Mater. Chem. B 5 (2017) 3836-3841

[30] Y.Q. Xu, B.H. Li, L.L. Xiao, J. Ouyang, S.G. Sun, Y. Pang, A colorimetric and near-infrared fluorescent probe with high sensitivity and selectivity for acid phosphatase and inhibitor screening, Chem. Commun. 50 (2014) 8677-8680.

[31] H.D. Li, Q.C. Yao, J.L. Fan, J.J. Du, J.Y. Wang, X.J. Peng, A two-photon NIR-to-NIR fluorescent probe for imaging hydrogen peroxide in living cells, Biosens. Bioelectron. 94 (2017) 536-543.

[32] X.M. Wu, A.D. Shao, S.Q. Zhu, Z.Q. Guo, W.H. Zhu, A novel colorimetric and ratiometric NIR fluorescent sensor for glutathione based on dicyanomethylene-4H-pyran in living cells, Sci. China Chem. 59 (2015) 62-69.

[33] B.X. Shen, Y. Qian, Z.Q. Qi, C.G. Lu, Q. Sun, X. Xia, Y.P. Cui, Near-infrared BODIPY-based two-photon ClO− probe based on thiosemicarbazide desulfurization reaction: naked-eye detection and mitochondrial imaging, J. Mater. Chem. B 5 (2017) 5854-5861.

[34] Q. Jin, L. Feng, D.D. Wang, J.J. Wu, J. Hou, Z.R. Dai, S.G. Sun, J.Y. Wang, G.B. Ge, J.N. Cui, L. Yang, A highly selective near-infrared fluorescent probe for carboxylesterase 2 and its bioimaging applications in living cells and animals, Biosens. Bioelectron. 83

(2016) 193-199.

[35] Z.W. Gao, J.Y. Sun, M. Gao, F.B. Yu, L.X. Chen, Q.G. Chen, A unique off-on near-infrared cyanine-based probe for imaging of endogenous alkaline phosphatase activity in cells and in vivo, Sens. Actuator B-Chem. 265 (2018) 565-574.

[36] J. Zhang, C. Li, R. Zhang, F. Zhang, W. Liu, X. Liu, S.M.-Y. Lee, H. Zhang, A phosphinate-based near-infrared fluorescence probe for imaging the superoxide radical anion in vitro and in vivo, Chem. Commun. 52 (2016) 2679-2682.

[37] Y. Tang, A.D. Shao, J. Cao, H. Li, Q. Li, M.Y. Zeng, M. Liu, Y.S. Cheng, W.H. Zhu, cNGR-based synergistic-targeted NIR fluorescent probe for tracing and bioimaging of pancreatic ductal adenocarcinoma, Sci. China Chem. 61 (2017) 184-191.

[38] H. Chen, B.L. Dong, Y.H. Tang, W.Y. Lin, A unique "integration" strategy for the rational design of optically tunable near-infrared fluorophores, Acc. Chem. Res. 50 (2017) 1410-1422.

[39] E. Camerino, G.C. Daniels, J.H. Wynne, E.B. Iezzi, Synthesis and kinetics of disassembly for silyl-containing ethoxycarbonyls using fluoride ions, RSC Adv. 8 (2018) 1884-1888.

[40] Y. Zhou, M.M. Liu, J.Y. Li, M.A. Ye, C. Yao, Fluorescence turn-on detection of fluoride using HPQ-silyl ether reactive probes and its in vivo application, Dyes Pigments 158 (2018) 277-284.

[41] Y.J. Li, Q. Sun, L. Su, L.L. Yang, J. Zhang, L. Yang, B.H. Liu, C.L. Jiang, Z.P. Zhang, A single nanofluorophore "turn on" probe for highly sensitive visual determination of environmental fluoride ions, RSC Adv. 8 (2018) 8688-8693.

[42] C.M. Lopez-Alled, A. Sanchez-Fernandez, K.J. Edler, A.C. Sedgwick, S.D. Bull, C.L. McMullin, G. Kociok-Kohn, T.D. James, J. Wenk, S.E. Lewis, Azulene-boronate esters: colorimetric indicators for fluoride in drinking water, Chem. Commun. 53 (2017) 12580-12583.

[43] Y.M. Shen, X.Y. Zhang, Y.Y. Zhang, H.T. Li, Y.D. Chen, An ICT-Modulated strategy to construct colorimetric and ratiometric fluorescent sensor for mitochondria-targeted fluoride ion in cell living, Sens. Actuator B-Chem. 258 (2018) 544-549.

[44] B.H. Choi, J.H. Lee, H. Hwang, K.M. Lee, M.H. Park, Novel dimeric o-carboranyl triarylborane: intriguing ratiometric color-tunable sensor via aggregation-induced emission by fluoride anions, Organometallics 35 (2016) 1771-1777.

[45] Q.Y. Yang, C.M. Jia, Q. Chen, W. Du, Y.L. Wang, Q. Zhang, A NIR fluorescent probe for the detection of fluoride ions and its application in in vivo bioimaging, J. Mater. Chem. B 5 (2017) 2002-2009.

[46] S. Jiao, X.C. Wang, Y.H. Sun, L.J. Zhang, W.L. Sun, Y. Sun, X.H. Wang, P.Y. Ma, D.Q. Song, A novel fluorescein-coumarin-based fluorescent probe for fluoride ions and its applications in imaging of living cells and zebrafish in vivo, Sens. Actuator B-Chem. 262 (2018) 188-194.

[47] S.D. Liu, L.W. Zhang, P.P. Zhou, Y. Yang, W.S. Wu, Distinctive fluoride fluorescent probes with ratiometric characteristics combinate desilylation, hydrogen bond and ESIPT process: spectral and mechanistic studies, Sens. Actuator B-Chem. 255 (2018) 401-407.

[48] P.L. Liu, B.W. Li, C.Y. Zhan, F. Zeng, S.Z. Wu, A two-photon-activated prodrug for therapy and drug release monitoring, J. Mater. Chem. B 5 (2017) 7538-7546.

Figure Captions

Scheme 1. Schematic illustration of DCM-Si based NIR fluorescence probe for detection of F^- in vitro an in vivo.

Scheme 2. The synthesis method of probe DCM-Si.

Fig. 1. Time-dependent absorption spectra of DCM-Si (5 μM) with 100 μM F^- in aqueous solution (DMSO/water = 95/5, v/v). Inset: Photos of DCM-Si solution before and after addition of F^- with the range of time.

Fig. 2. Time-dependent emission spectra of DCM-Si (5 μM) with 100 μM F^- in aqueous solution (DMSO/water = 95/5, v/v). Inset: Photos of DCM-Si solution before and after addition of F^- with the range of time under the excitation of 365 nm UV light (left); plot relative intensity at 665 nm versus time for DCM-Si (5 μM) solution upon addition of 100 μM F^- (right).

Fig. 3. Emission spectra of DCM-Si (5 μM) in aqueous solution (DMSO/water = 95/5, v/v) upon the addition various concentrations of F^- (from 0 to 100 μM). Inset: plot relative intensity at 665 nm for DCM-Si (5 μM) solution versus F^- concentration (0-100 μM).

Fig. 4. Linear relationship between the relative intensity at 665 nm ($F-F_0$) and F^- concentration (1-40 μM).

Fig. 5. Fluorescence emission spectra of DCM-Si (5 μM) in aqueous solution (DMSO/water =

95/5, v/v) with F^- (100 μM) and free various interfering analytes (Cl^-, Br^-, I^-, AcO^-, HSO_4^-, $H_2PO_4^-$, NO_3^-, and OH^-, 100 μM), and coexistence of F^- and various interfering ions including Cl^-, Br^-, I^-, AcO^-, HSO_4^-, $H_2PO_4^-$, NO_3^-, and OH^-.

Fig. 6. HPLC chromatogram analysis of DCM-NH_2 (5 μM), DCM-Si (5 μM), and DCM-Si (5 μM) + F^- (100 μM). Solvent ratio was acetonitrile/water = 90/10.

Fig. 7. Frontier molecular orbital profiles of DCM-Si and DCM-NH_2 based on DFT (B3LYP/6-31G*) calculations.

Fig. 8. Confocal microscopy images of DCM-Si (10 μM) in HeLa cells. The cells were incubated with only DCM-Si (10 μM) for 60 min as control (A). The cells were incubated with 50 μM (B), or 100 μM (C) F^- for 60 min, and further incubated with DCM-Si (10 μM) for 60 min as experimental groups.

Fig. 9. Fluorescence microscope images of DCM-Si (10 μM) in zebrafish. The zebrafishes were incubated with only DCM-Si (10 μM) for 60 min as control (A). The zebrafishes were incubated with 50 μM (B), or 100 μM (C) F^- for 60 min, and further incubated with DCM-Si (10 μM) for 60 min as experimental groups.

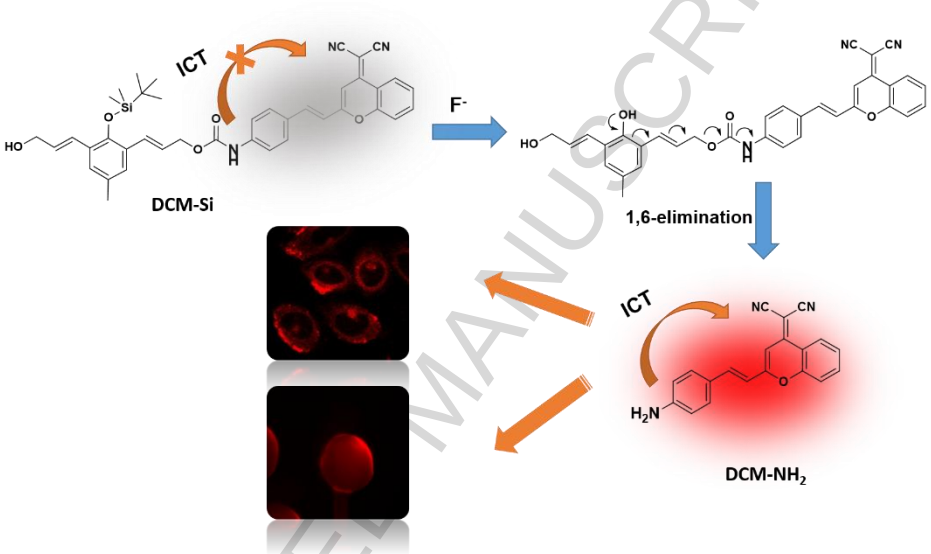

Scheme 1

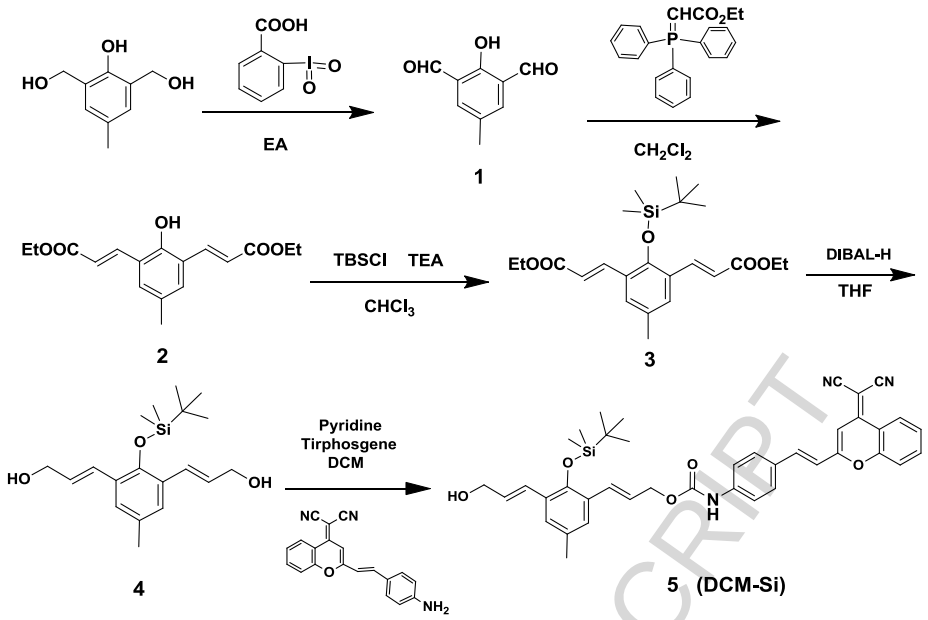

Scheme 2

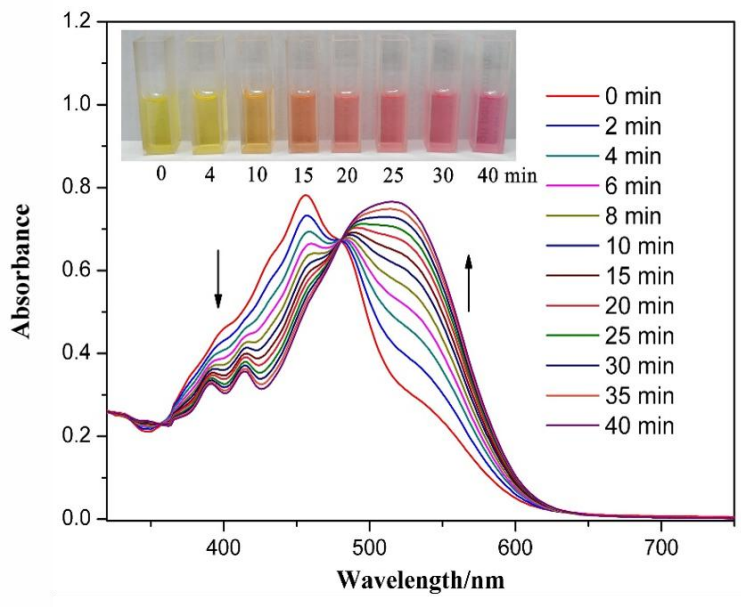

Figure 1

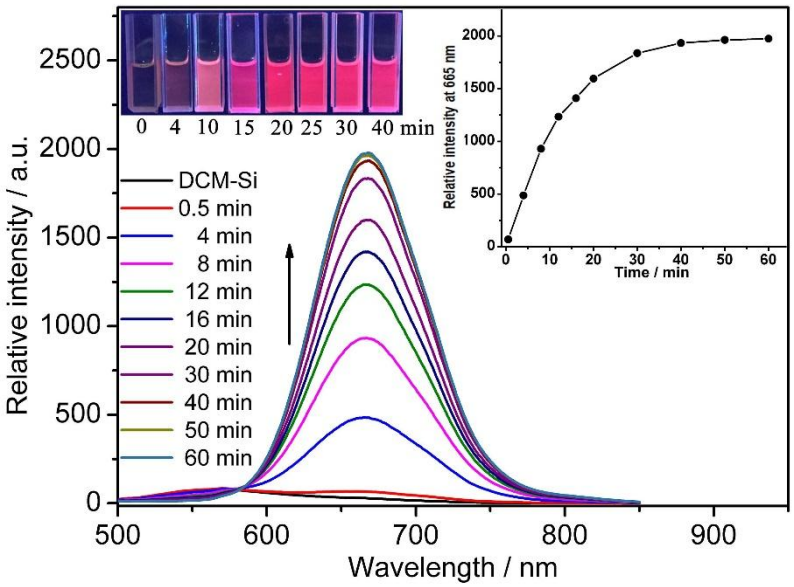

Figure 2

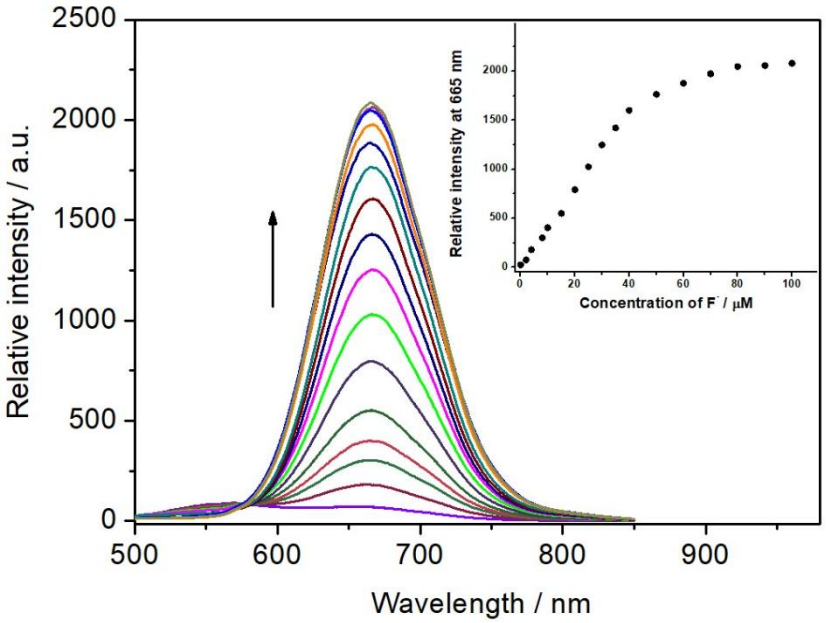

Figure 3

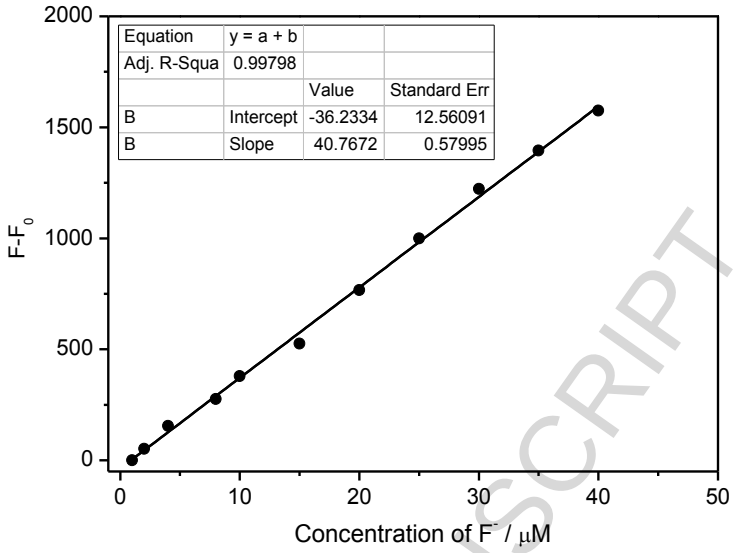

Figure 4

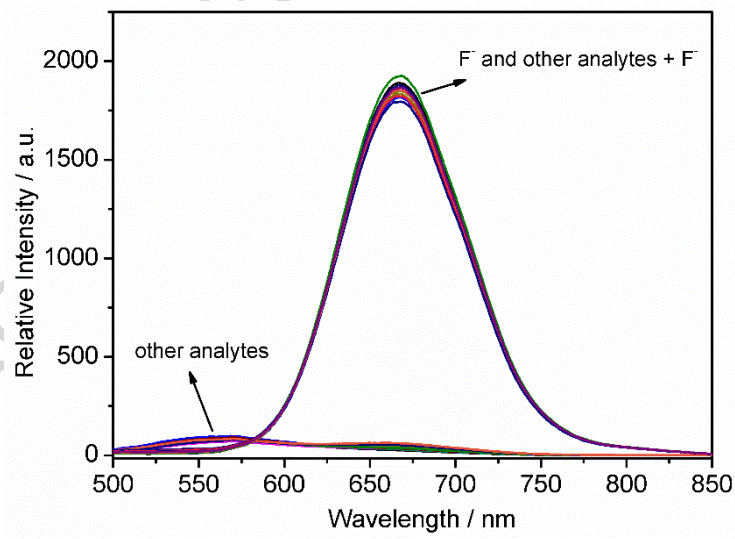

Figure 5

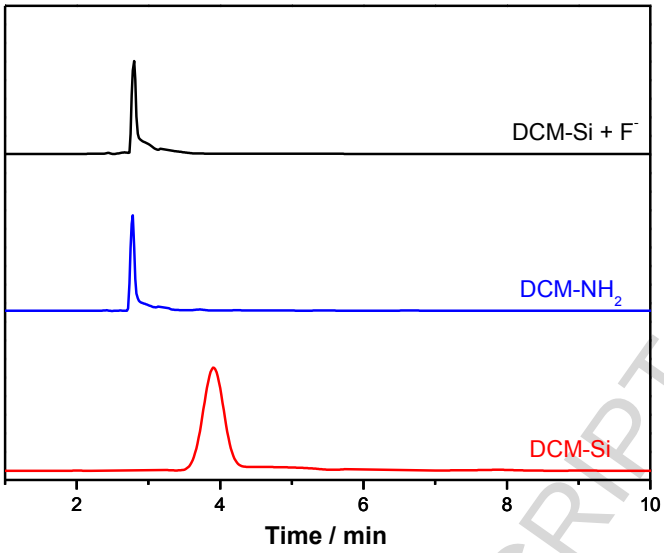

Figure 6

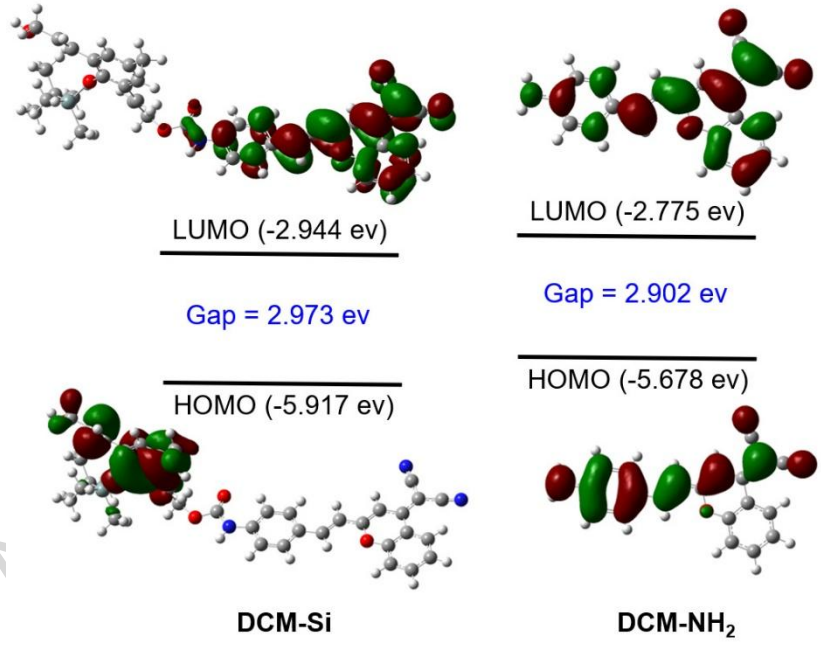

Figure 7

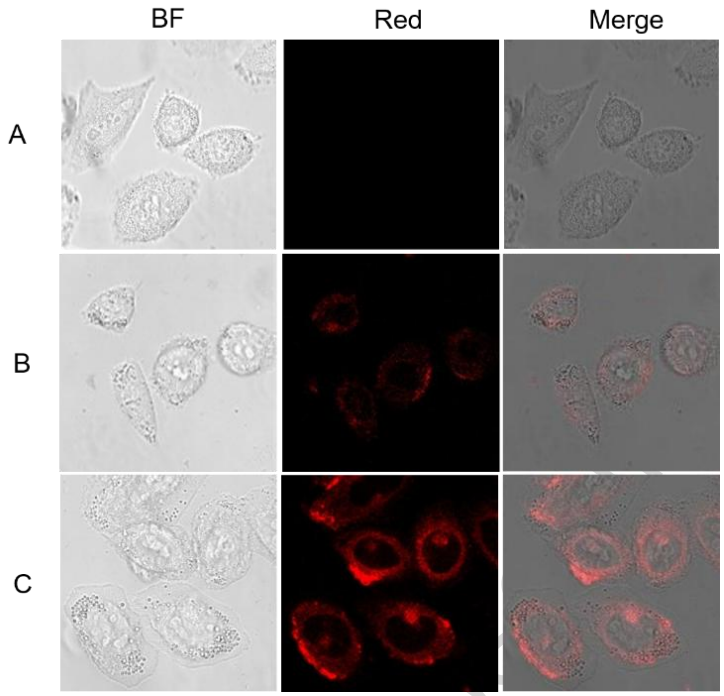

Figure 8

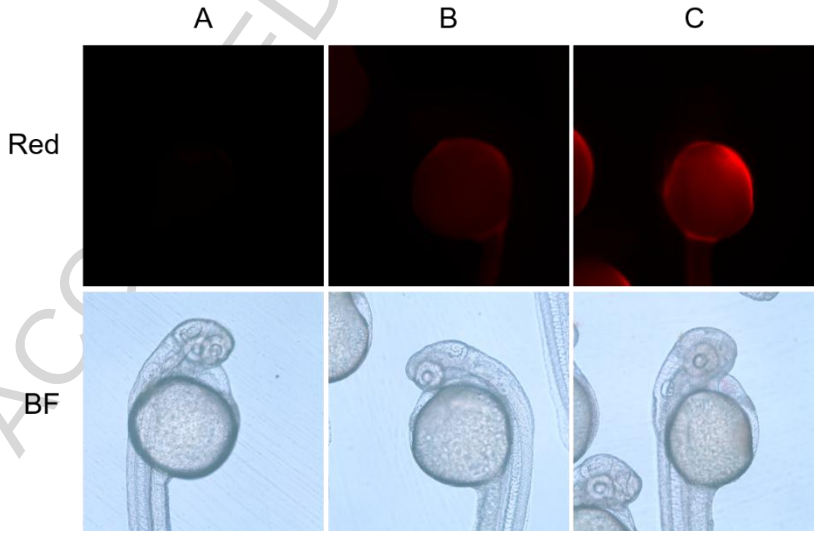

Figure 9

TOC:

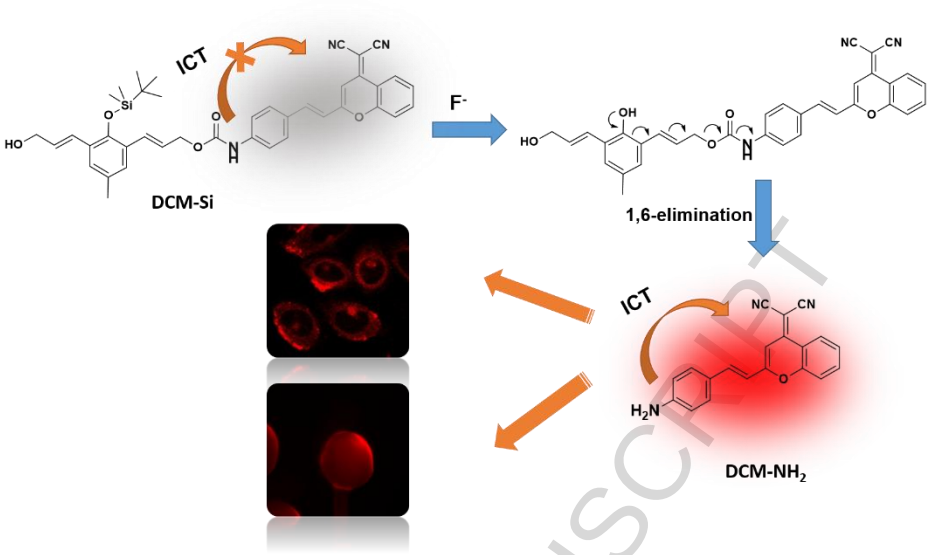

A new NIR fluorescent probe (DCM-Si) was designed and synthesized for specific lighting up F^- in living cells and bodies. DCM-Si exhibits almost no fluorescent emission in terms of ICT block from the amino group of DCM-NH_2. The NIR fluorescent emission of DCM-Si was successfully activated by the fluoride ions in HeLa cells and zebrafish through the fluorescence imaging.

Highlights:

1. A novel NIR fluorescent probe was synthesized.
2. The probe was specific and sensitive lighting up F^- in solution.
3. Emission evolution was obtained by adding F^- in living cells and zebrafishes.